



Article

# Andean Sacha Inchi (*Plukenetia Volubilis* L.) Leaf-Mediated Synthesis of Cu<sub>2</sub>O Nanoparticles: A Low-Cost Approach

Brajesh Kumar <sup>1,2,\*</sup> , Kumari Smita <sup>2</sup>, Alexis Debut <sup>2</sup>  and Luis Cumbal <sup>2</sup>

<sup>1</sup> Post Graduate Department of Chemistry, TATA College, Kolhan University, Chaibasa, Jharkhand 833202, India

<sup>2</sup> Centro de Nanociencia y Nanotecnología, Universidad de las Fuerzas Armadas ESPE, Av. Gral. Rumiñahui s/n, Sangolqui P.O. BOX 171-5-231B, Ecuador; kumarismi@gmail.com (K.S.); apdebut@espe.edu.ec (A.D.); lhcumbal@espe.edu.ec (L.C.)

\* Correspondence: krmbraj@gmail.com; Tel.: +91-8757618562

Received: 9 May 2020; Accepted: 4 June 2020; Published: 6 June 2020



**Abstract:** In this work, Andean sachu inchi (*Plukenetia volubilis* L.) leaves were used to prepare monodispersed cuprous oxide (Cu<sub>2</sub>O) nanoparticles under heating. Visual color changes and UV-visible spectroscopy of colloidal nanoparticles showed  $\lambda_{\text{max}}$  at 255 nm, revealing the formation of copper oxide nanoparticles. Transmission electron microscopy and dynamic light scattering analysis indicated that the prepared nanoparticles were spherical with an average size of 6–10 nm. The semi-crystalline nature and Cu<sub>2</sub>O phase of as-prepared nanoparticles were examined by X-ray diffraction. Fourier-transform infrared spectroscopy confirmed the presence of polyphenols, alkaloids and sugar in the sachu inchi leaf, allowing the formation of Cu<sub>2</sub>O nanoparticles from Cu<sup>2+</sup>. Additionally, as-synthesized Cu<sub>2</sub>O nanoparticles exhibited good photocatalytic degradation activity against methylene blue (>78%, 150 min) with rate constant 0.0219106 min<sup>-1</sup>. The results suggested that the adopted method is low-cost, simple, ecofriendly and highly selective for the synthesis of small Cu<sub>2</sub>O nanoparticles and may be used as a nanocatalyst in the future in the efficient treatment of organic pollutants in water.

**Keywords:** *Plukenetia volubilis*; green synthesis; Cu<sub>2</sub>O nanoparticles; XRD; catalysis

## 1. Introduction

During the last two decades, nanoparticles/nanomaterials (of size less than 100 nm) have been extensively studied due to their exclusive properties such as high surface-to-volume ratio, flexibility, quantum size, high yield strength, rigidity, ductility and macro-quantum tunneling effect, and are currently used in various areas of chemistry, physics, medicine and engineering [1,2]. Copper is one of the most important elements used worldwide for various purposes. In particular, copper oxide nanoparticles have received great attention because of their low cost, high yield, mild reaction conditions and fantastic applications in batteries [3], catalysis [4], optical devices [5], printed electronics [6], anticancer therapeutics, sensing, antioxidants [7], antimicrobial activities [8], fuel cells [9], bioimaging [10], dye removal [11], gas sensors [12], etc.

Copper oxide nanoparticles have been synthesized by a variety of chemical and physical methods including hydrothermal synthesis [13], the wet chemical method [14], solution phase synthesis [15], sonochemical synthesis [16], the microwave method [17], the laser ablation method [18] and ball milling [19], in which a large amount of solvents is required for obtaining pure and well-defined nanoparticles. They create various problems for the ecosystem and the environment [7,20]. Plant-based metal nanoparticle preparation methods are low-cost, simple and ecofriendly and hold great promise

in biotechnology applications due to the presence of effective reducing and capping agents such as carbohydrates, polyphenols, terpenoids, sugars, amino acids, flavanoids, saponins, etc. [20]. Therefore, they are favored over chemical and physical synthesis methods [21]. Previously reported syntheses of cuprous oxide/cupric oxide ( $\text{Cu}_2\text{O}/\text{CuO}$ ) nanoparticles have used plant materials to support large-scale synthesis, including extracts of *Azadirachta indica* leaf [22], *Aegle Marmelo* leaf [23], *Aloe barbadensis* Miller leaf [24], *Acalypha indica* leaf [25] *Punica granatum* peel [26], *Terminalia arjuna* bark [27], *Stachys lavandulifolia* flower [28], *Terminalia bellirica* [29] and *Rubus glaucus* fruit [30], etc.

Sacha inchi (SI) (*Plukenetia volubilis* L.) is a promising crop plant originally from the Amazon basin of Latin America. Its star-shaped green fruits produce nut-like seeds with a bitter taste and have been consumed by humans since Incan times due to their high content of fatty acids ( $\omega$ -3 and  $\omega$ -6, 35–60%), protein (27–33%), carbohydrates and antioxidants [31]. Its dried leaves are marketed as a tea and contain 84.2–93.4% sugar [32]. Phytochemicals such as saponins, terpenoids, polyphenolic compounds (flavonoids) and other components are also found in SI leaves and are responsible for their antioxidant and antiproliferative activities [33].

Thus, the utilization of these lost crops in nanotechnology and green chemistry has been continued by our group: SI leaves for the synthesis of silver nanoparticles [34], SI oil for the synthesis of silver [35] and gold nanoparticles [36] and SI shell biomass for the synthesis of silver nanoparticles [37] and removal of  $\text{Cu}^{2+}/\text{Pb}^{2+}$  [38]. Our research on the SI plant may support an additional source of revenue for farmers on the western and northern edges of South America, such as Colombia, Ecuador, Venezuela, Peru, Bolivia, Brazil and Suriname, and in the Lesser Antilles [31].

To our knowledge, there have been no reports of the synthesis of  $\text{Cu}_2\text{O}$  nanoparticles using the SI leaf. Herein, green  $\text{Cu}_2\text{O}$  nanoparticles were synthesized by reducing  $\text{Cu}^{2+}$  ions with aqueous extract of SI leaf. This nanoparticle is used in the degradation of methylene blue (MB), one of the most common organic pollutants in wastewater from the dye industry (Figure 1). It is environmentally undesirable at a trace level and excessive usage of MB causes serious diseases in human beings [35,36]. Hence, the development of an ecofriendly method for the removal of MB from wastewater is necessary. In this work, full spectroscopic and microscopic characterizations were performed to confirm the formation of  $\text{Cu}_2\text{O}$  nanoparticles. Photocatalytic evaluation experiments indicated that  $\text{Cu}_2\text{O}$  nanoparticles possess fast catalytic activity in the degradation of MB.

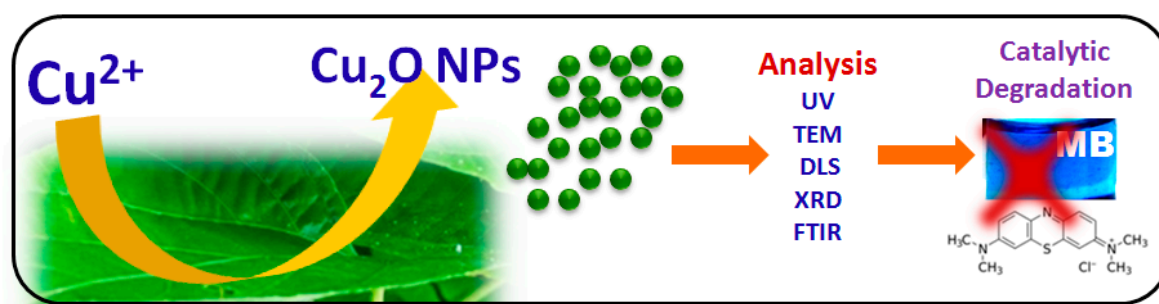


**Figure 1.** Schematic presentation of the synthesis and application of  $\text{Cu}_2\text{O}$  nanoparticles.

## 2. Materials and Methods

### 2.1. Materials

Copper nitrate ( $\text{Cu}(\text{NO}_3)_2 \cdot 3\text{H}_2\text{O}$ , 99.0%) and methylene blue (MB, 99.5%) were purchased from Spectrum, USA. Sacha inchi (SI) leaves were collected with the help of Mr. Abraham Rodolfo Sanchez Piñuela from a farm in Quito, Ecuador. Milli-Q water was used in all experiments. All chemicals listed above were of analytical grade and used without any purification.

## 2.2. Preparation of Cu<sub>2</sub>O Nanoparticles

Thoroughly washed SI leaves were shade-dried for one week. The extraction of phytochemicals from the SI leaves was performed by an earlier extraction method [34]. Nearly 800 mg of the dried SI leaf was crushed into small pieces and transferred to a 100 mL flask containing 50 mL of Milli-Q water, and then it was mixed well and heated (64–68 °C) for 30 min. The obtained red extract of SI leaf was filtered through Whatman No. 1 paper and stored at 4 °C for further use. For the synthesis of Cu<sub>2</sub>O nanoparticles, 5 mL of SI leaf extract was added slowly to 20 mL of Cu(NO<sub>3</sub>)<sub>2</sub> solution (10 mM), followed by heating for 5 h at 85–90 °C with continuous stirring. The formation of the Cu<sub>2</sub>O nanoparticles was indicated by a change of reaction mixture color from bluish-red to a greenish color.

## 2.3. Characterization of Cu<sub>2</sub>O Nanoparticles

The samples containing nanoparticles were confirmed by a UV-visible spectrophotometer, GENESYS™ 8 from Thermo Spectronic, England. The particle size distribution of the sample was analyzed using the HORIBA, DLS Version LB-550 program, Japan. The morphology and selected area electron diffraction (SAED) pattern of the nanoparticles were captured on a transmission electron microscope (TEM), FEI Tecnai, G2 Spirit Twin, Holland. X-ray diffraction (XRD) studies on thin films of the nanoparticle were carried out using a PANalytical brand  $\theta$ -2 $\theta$  configuration (generator-detector) X-ray tube, copper  $\lambda = 1.54059 \text{ \AA}$ , and an EMPYREAN diffractometer. The Fourier-transform infrared (FTIR) spectra were collected on a Spectrum Two IR spectrometer from Perkin Elmer, USA. The samples for FTIR and XRD analysis were prepared by carefully depositing a thin film of Cu<sub>2</sub>O nanoparticles on a glass slide by injecting and heating 1800  $\mu\text{L}$  (600  $\mu\text{L} \times 3$  times) of Cu<sub>2</sub>O solution drop by drop at 60–65 °C for 20–30 min allowing the solvent to evaporate. After that, the thin film of the samples was scratched and the FTIR-ATR analysis was performed.

## 2.4. Photocatalytic Effects

The photocatalytic activity of Cu<sub>2</sub>O nanoparticles during the degradation of MB was determined by carrying out the reaction in direct sunlight (1040–1165 cd/m<sup>2</sup>) at 30–35 °C (atmospheric temperature). Typically, 5 mL MB (10 mg/L) was mixed with 1 mL H<sub>2</sub>O in a glass tube; in a second glass tube, 5 mL MB (10 mg/L), aqueous solution containing Cu<sub>2</sub>O nanoparticles (500  $\mu\text{L}$ ) and H<sub>2</sub>O (500  $\mu\text{L}$ ) was mixed in the dark for 20 min to reach an adsorption-desorption equilibrium. Then, both sets were exposed to direct sunlight and the progress of the degradation reaction was monitored at different time intervals by UV-vis spectroscopy at a wavelength of 664 nm. To evaluate the interference of SI leaf extract on the reduction of MB, a separate reaction was performed in which 5 mL of MB (10 mg/L) was mixed with 500  $\mu\text{L}$  of SI extract and 500  $\mu\text{L}$  of H<sub>2</sub>O. After that, the reaction mixture was heated at 40 °C for 120 min in the dark. The photocatalytic degradation percentage of MB was calculated using Equation (1) and the respective first-order rate constants (k) according to Equation (2).

$$\eta = (A_0 - A_t)/A_0 \times 100\% \quad (1)$$

$$kt = \ln (A_0/A_t) \quad (2)$$

where  $\eta$  is the rate of degradation of MB in terms of percentage,  $A_0$  is the initial absorbance of the dye solution and  $A_t$  is the absorbance of the MB at time  $t$ , respectively.  $C_0/C_t$  is measured from the relative intensity of absorbance ( $A_0/A_t$ ). The linear relationship of  $\ln (A_0/A_t)$  versus time indicates that the photodegradation of MB follows first-order kinetics [35,36].

### 3. Results and Discussion

#### 3.1. UV-Vis Spectroscopy Analysis

Figure 2 shows the UV-visible absorption spectra of as-prepared  $\text{Cu}_2\text{O}$  nanoparticles in the presence of SI leaf extract in an aqueous medium. The colorimetric reduction reaction of  $\text{Cu}^{2+}$  ions with the SI leaf extract (red colour) indicated the formation of a greenish-colored solution (a and b in Figure 2), attributed to the surface plasmon resonance (SPR) of the  $\text{Cu}_2\text{O}$  nanoparticles [30,39]. The absorption peaks appearing at 260 and 340 nm (red line) correspond to the polyphenolic compounds present in the SI leaf extract [34], while as-prepared  $\text{Cu}_2\text{O}$  nanoparticles exhibited a broad absorption peak at between 240 to 380 nm having two  $\lambda_{\text{max}}$  at 255 and 360 nm (green line), respectively [39,40]. The change observed in the spectrum after the reduction of  $\text{Cu}^{2+}$  ions to  $\text{Cu}_2\text{O}$  nanoparticles corresponds to the formation of Cu-phytochemicals, complex or spherical  $\text{Cu}_2\text{O}$  nanoparticles with size 2–5 nm and quite stable in the shape-position of absorption after one month, indirectly indicating the stability of the nanoparticles [39,40].

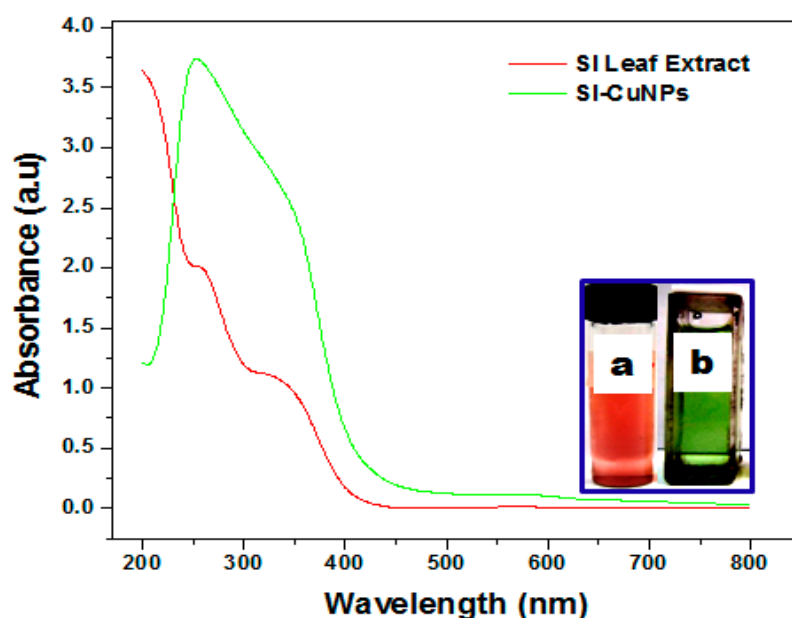


**Figure 2.** UV-vis spectra of SI leaf extract (red line) and  $\text{Cu}_2\text{O}$  nanoparticles (green line). Visual picture of solution containing (a) SI leaf extract and (b)  $\text{Cu}_2\text{O}$  nanoparticles.

#### 3.2. TEM and SAED Analysis

The exact shape and size of the nanoparticles was determined using a TEM image. The high- (Figure 3a) and low- (Figure 3d) magnification TEM images showed a good dispersion with the spherical morphology of  $\text{Cu}_2\text{O}$  nanoparticles inside the SI leaf extract. The majority of the nanoparticles observed from the TEM micrograph are small, with a size of 6–10 nm, indicating the availability of high surface catalytic activity for  $\text{Cu}_2\text{O}$  nanoparticles; a small few of the  $\text{Cu}_2\text{O}$  nanoparticles are of a bigger size, around 20–45 nm. This may be due to the presence of excessive SI phytochemicals on the surface of the  $\text{Cu}_2\text{O}$  nanoparticles, which can cause the aggregation and enlargement of nanoparticles during the synthesis of  $\text{Cu}_2\text{O}$  nanoparticles. The size distribution pattern of the nanoparticles observed in the TEM image (Figure 3a) was analyzed manually using ImageJ software. It showed the average size of the  $\text{Cu}_2\text{O}$  nanoparticles to be  $6.67 \pm 3.96$  nm (Figure 3b). No aggregation of nanoparticles suggested the presence of hydrophobic coating around the  $\text{Cu}_2\text{O}$  nanoparticles. The SAED pattern of the  $\text{Cu}_2\text{O}$  nanoparticles (Figure 3c) shows partial concentric rings which signify that the particles are spherical shape, semicrystalline nature and indexed as (111) and (200) lattice planes for the face-centred cubic (FCC) structure of  $\text{Cu}_2\text{O}$  nanoparticles [16].

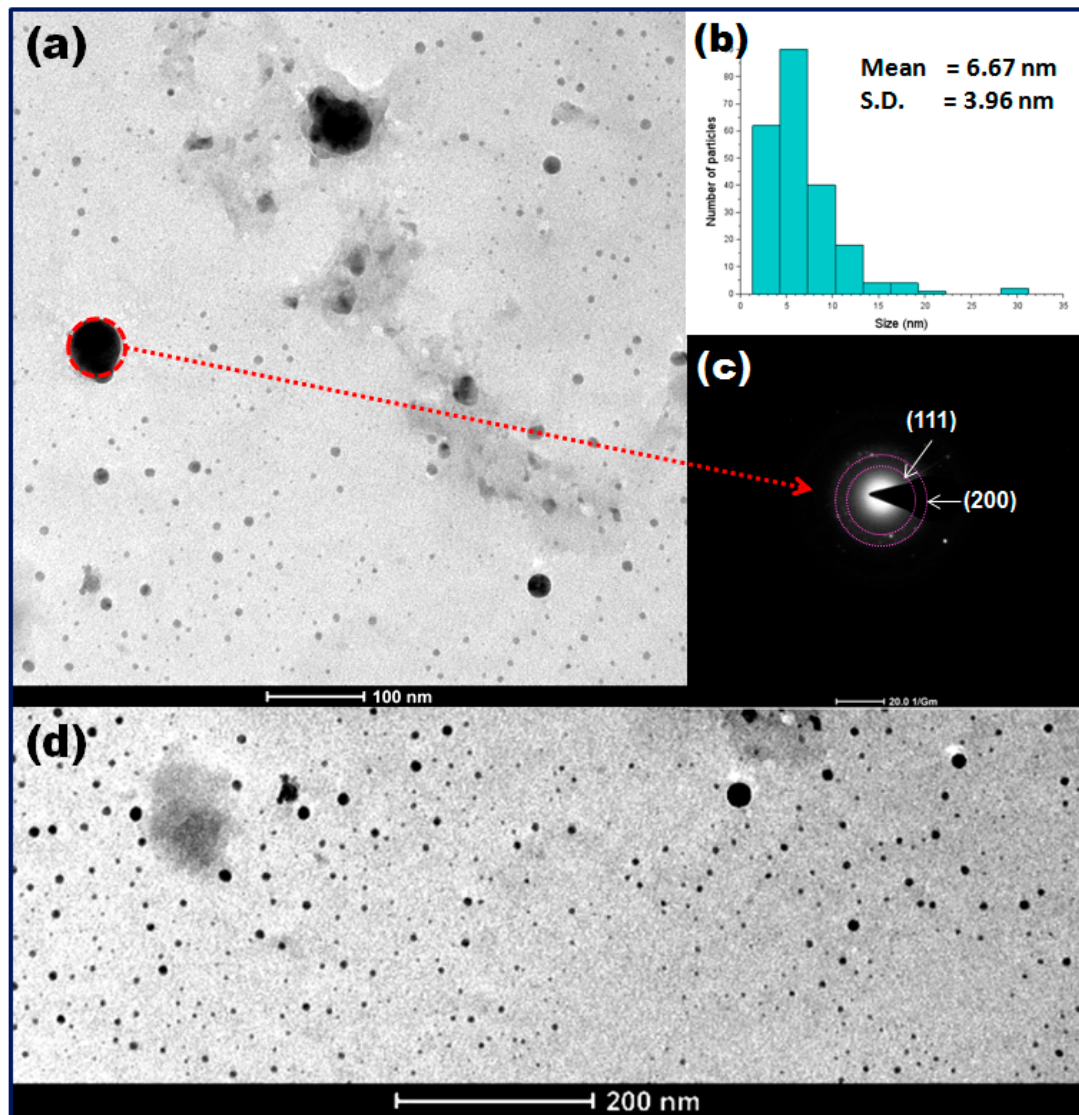


**Figure 3.** (a,d) TEM (transmission electron microscope) images of  $\text{Cu}_2\text{O}$  nanoparticles synthesized in solution, (b) size distribution pattern and (c) SAED pattern.

### 3.3. DLS Analysis

The dynamic light scattering (DLS) technique gives valuable information about the hydrodynamic size distribution of the  $\text{Cu}_2\text{O}$  nanoparticles (Figure 4). The average width of the  $\text{Cu}_2\text{O}$  nanoparticles was found to be  $8.2 \pm 2.1$  nm with polydispersity index (PDI) = 0.0656. The observed PDI < 0.1 clearly indicates that the synthesized  $\text{Cu}_2\text{O}$  nanoparticles were monodispersed in nature [29]. However, the average size of as-synthesized  $\text{Cu}_2\text{O}$  nanoparticles determined by the DLS method was slightly higher than in the TEM analysis. This is due to either the presence of organic coating around nanoparticles or the screening of small particles by bigger ones [36,41].



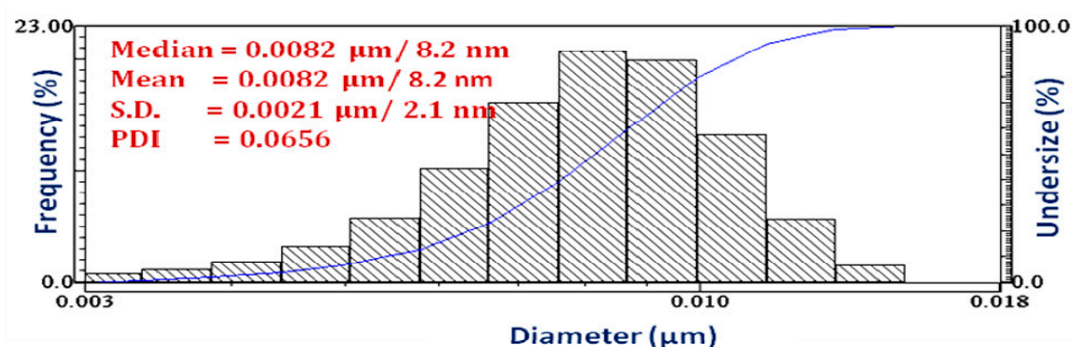


**Figure 4.** DLS size distribution of the  $\text{Cu}_2\text{O}$  nanoparticles. Abbreviations: DLS, dynamic light scattering.

### 3.4. XRD Analysis

In order to clarify the nature and crystallinity of the  $\text{Cu}_2\text{O}$  nanoparticles, XRD analysis was performed as shown in Figure 5. The presence of intense peaks at  $2\theta = 36.46$  and  $42.45^\circ$  represents the (111) and (200) planes. The XRD reflections of  $\text{Cu}_2\text{O}$  match that of Inorganic Crystal Structure Database ICDD (Inorganic Crystal Structure Database) no. 98-018-0846 corresponding to the semi-crystalline cubic FCC structure, which match the common peaks in the earlier report [42]. It can be also observed that the undesired peak at  $2\theta = 32^\circ$  is due to a typical impurity caused by a metallo-organic structure [23,24]. It is likely that these peaks indicate that the phytochemicals in SI leaf extract attached to the  $\text{Cu}_2\text{O}$  nanoparticles and were also involved with surface-capped nanoparticles. However, the observed size of the nanoparticles in the XRD using the Scherrer formula ( $\sim 46$  nm) is bigger than in the TEM-DLS results [40]; this may be due to the aggregation of particles during drying for the preparation of XRD samples. This increment could be attributed to the light scattering effect because of the aggregation of the metal [43].

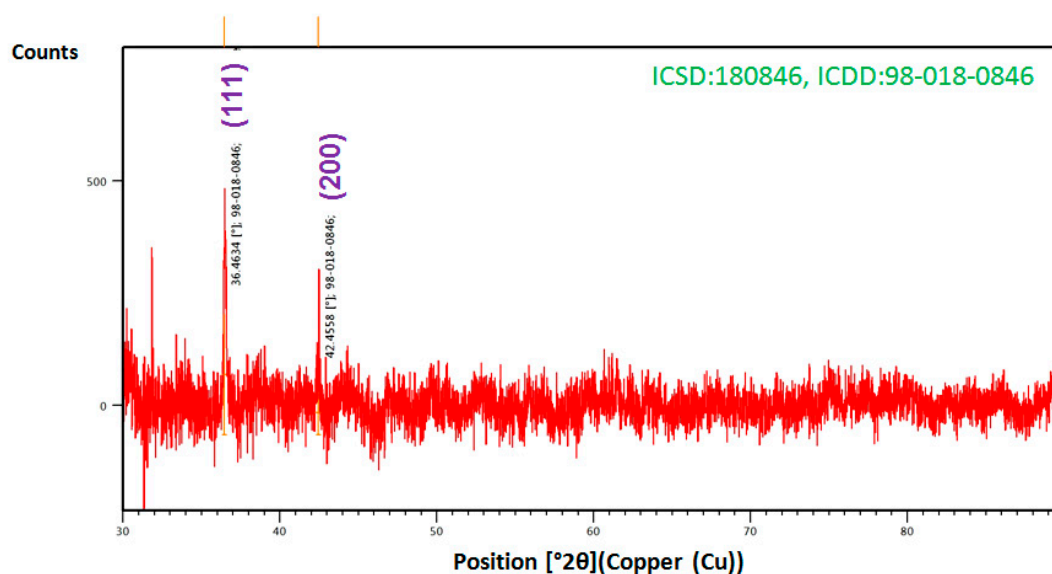


**Figure 5.** XRD pattern of the  $\text{Cu}_2\text{O}$  nanoparticles. Abbreviations: XRD, X-ray diffraction.

### 3.5. FTIR Analysis

FTIR spectra of the particles were recorded to detect the chemical interaction between SI leaf extract and  $\text{Cu}^{2+}$  that occurs during the synthesis of  $\text{Cu}_2\text{O}$  nanoparticles (Figure 6). They reveal a weak absorption band at  $698\text{ cm}^{-1}$  may correspond to the Cu-O bond vibrational frequencies, which are slightly higher than reported Cu-O ( $645\text{ cm}^{-1}$ ) bond vibration due to depending on the degree of hydrogen bonding. Furthermore, the additional Cu-O-H bonds lead to bending absorptions in the

region of  $896\text{ cm}^{-1}$  [44]. This can be attributed to the presence of the Cu–O bond. The strong band at  $1028\text{ cm}^{-1}$  can be attributed to the C–O–C/secondary C–OH bonds in the polysaccharide/protein structure of the SI leaf [34]. The prominent bands at around 1241, 1314, 1374 and  $1601\text{ cm}^{-1}$  can be attributed to the vibrational mode for C–H, C–N, C=C and C=O (amide 1) [30]. The existence of the peaks at 2847 and  $2921\text{ cm}^{-1}$  is due to the symmetric and asymmetric C–H stretching vibrations of flavonoids/phenolic compounds, respectively. The broad absorption peak at  $3331\text{ cm}^{-1}$  shows the existence of O–H/N–H stretching groups of macromolecular association [32,34]. The FTIR results indicate that the extract of SI leaf acted as a reducing and capping agent in the synthesis of the  $\text{Cu}_2\text{O}$  nanoparticles.

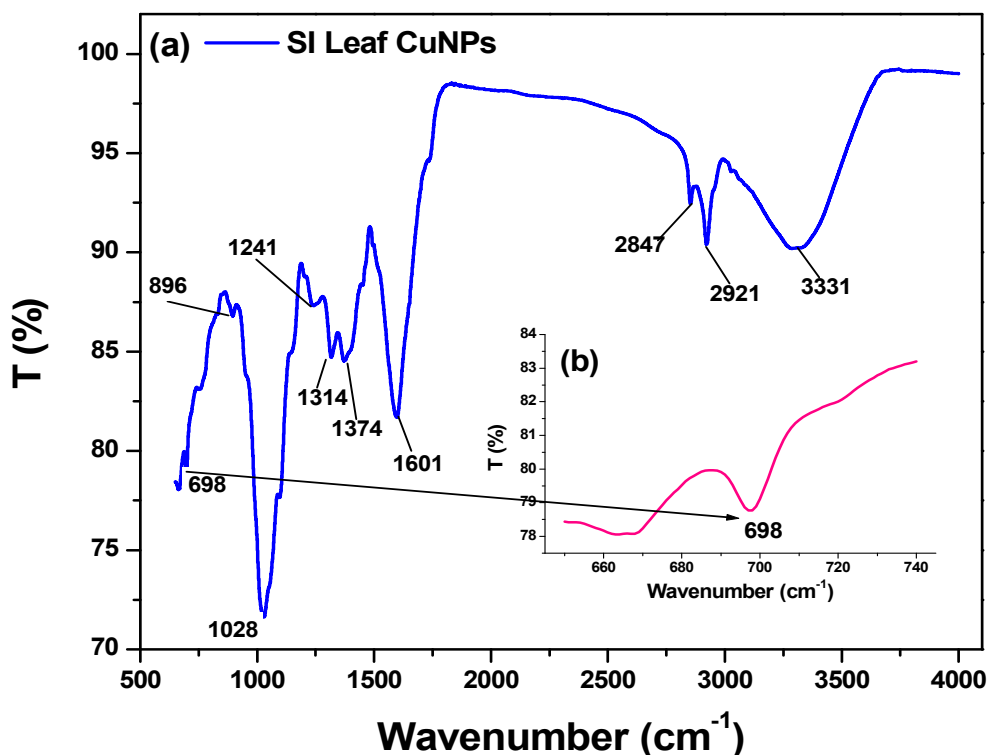


**Figure 6.** (a) FTIR spectrum of as-synthesized  $\text{Cu}_2\text{O}$  nanoparticles using SI leaf extract and (b) specific Cu–O at  $698\text{ cm}^{-1}$ .

### 3.6. Photocatalytic Activity

Figure 7a shows the photocatalytic activity of  $\text{Cu}_2\text{O}$  nanoparticles in the degradation of MB. The peaks at around 300 nm correspond to the absorption of the benzene ring and the peaks between 600–700 nm represent the absorption of heteropoly aromatic linkage of MB [45]. It can be seen that the degradation of MB increases with increasing solar irradiation time by observing the decrease in  $\lambda_{\text{max}}$  at 664 nm [35]. The photodegradation percentages ( $\eta$ ) of MB for 30, 75 and 150 min are 25.45%, 59.88% and 78.90% in the presence of  $\text{Cu}_2\text{O}$  nanoparticles when compared with that of the respective controls. No change of absorbance at  $\lambda_{\text{max}} = 664\text{ nm}$  was observed when a blank test was performed with MB and SI leaf extract. This confirms that the SI leaf extract does not interfere with the reduction of MB. In Figure 7b, the plots of  $\ln(A_0/A_t)$  versus time yield good linear correlations and are well fitted with pseudo-first-order kinetics. The result indicates that the observed rate constant ( $k$ ) and correlation coefficient ( $R^2$ ) for the MB degradation were  $21.9106 \times 10^{-3}\text{ min}^{-1}$  and 0.9999. Hence, the present study highlights the promising potential of SI leaf-synthesized  $\text{Cu}_2\text{O}$  nanoparticles for MB degradation in wastewater.

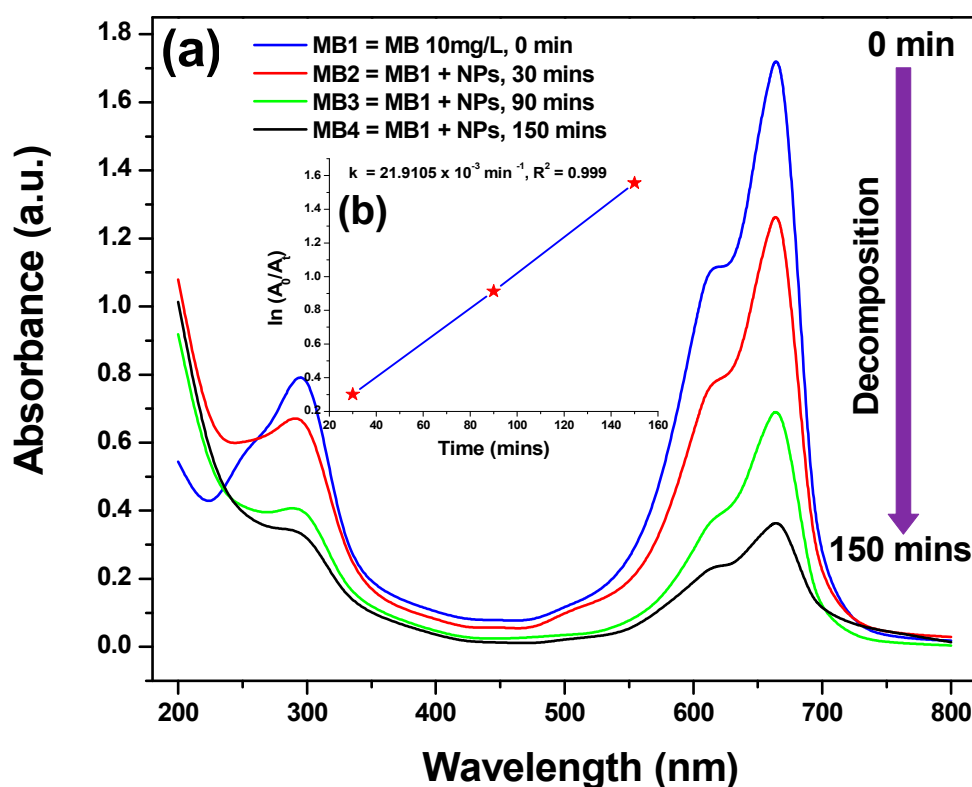


**Figure 7.** (a) Photocatalytic degradation pattern and (b)  $\ln(A_0/A_t)$  vs. time kinetic plot of MB using  $\text{Cu}_2\text{O}$  nanoparticles as photocatalyst.

#### 4. Conclusions

In conclusion, the use of SI leaf as a bioreductant for the synthesis of  $\text{Cu}_2\text{O}$  nanoparticles is a low-cost, simple and ecofriendly approach. The results obtained from DLS, TEM, XRD and FTIR suggest that the  $\text{Cu}_2\text{O}$  nanoparticles are highly dispersed, spherical, 6–10 nm in size, semicrystalline and surface-capped with SI leaf extract. The applied approach provided a  $\text{Cu}_2\text{O}$  nanocatalyst, which presented very good catalytic performance for the degradation of MB under sunlight.

**Author Contributions:** All authors contributed equally to the research work presented in this research article. All authors have read and agreed to the published version of the manuscript.

**Funding:** This scientific work has been funded by the Universidad de las Fuerzas Armadas ESPE and Prometeo Project of the National Secretariat of Higher Education, Science, Technology and Innovation (SENESCYT), Ecuador.

**Acknowledgments:** Many thanks to Principal (Kasturi Boipai), TATA College, Chaibasa, India for support to complete this research work.

**Conflicts of Interest:** The authors declare no conflict of interest.

#### References

- Din, M.I.; Arshad, F.; Hussain, Z.; Mukhtar, M. Green adeptness in the synthesis and stabilization of copper nanoparticles: Catalytic, Antibacterial, Cytotoxicity, and Antioxidant Activities. *Nanoscale Res. Lett* **2017**, *12*, 638. [[CrossRef](#)] [[PubMed](#)]
- Mehdizadeh, T.; Zamani, A.; Froushani, M.A. Preparation of Cu nanoparticles fixed on cellulosic walnut shell material and investigation of its antibacterial, antioxidant and anticancer effects. *Heliyon* **2020**, *6*, e03528. [[CrossRef](#)] [[PubMed](#)]
- Poizot, P.; Laruelle, S.; Grugeon, S.; Dupont, L.; Tarascon, J.M. Nano-sized Transition-Metal Oxides as Negative-Electrode Materials for Lithium-Ion Batteries. *Nature* **2000**, *407*, 496–499. [[CrossRef](#)] [[PubMed](#)]



4. Gawande, M.B.; Goswami, A.; Felpin, F.-X.; Asefa, T.; Huang, X.; Silva, R.; Zou, X.; Zboril, R.; Varma, R.S. Cu and Cu-based nanoparticles: Synthesis and applications in catalysis. *Chem. Rev.* **2016**, *116*, 3722–3811. [[CrossRef](#)]
5. Li, Y.; Qian, F.; Xiang, J.; Charles, M.L. Nanowire electronics and optoelectronics devices. *Mater. Today* **2006**, *9*, 18–27. [[CrossRef](#)]
6. Lee, W.; Lim, Y.S.; Kim, S.; Jung, J.; Han, Y.-K.; Yoon, S.; Piao, L.; Kim, S.-H. Crystal-to crystal conversion of Cu<sub>2</sub>O nanoparticles to Cu crystals and applications in printed electronics. *J. Mater. Chem.* **2011**, *21*, 6928–6933. [[CrossRef](#)]
7. Prasad, P.R.; Kanchi, S.; Naidoo, E.B. In-vitro evaluation of copper nanoparticles cytotoxicity on prostate cancer cell lines and their antioxidant, sensing and catalytic activity: One-pot green approach. *J. Photochem. Photobiol. B Biol.* **2016**, *161*, 375–382. [[CrossRef](#)]
8. Patel, B.H.; Channiwal, M.Z.; Chaudhari, S.B.; Mandot, A.A. Biosynthesis of copper nanoparticles; Its characterization and efficacy against human pathogenic bacterium. *J. Environ. Chem. Eng.* **2016**, *4*, 2163–2169. [[CrossRef](#)]
9. Xiao, G.; Gao, P.; Wang, L.; Chen, Y.; Wang, Y.; Zhang, G. Ultrasonochemical-assisted synthesis of CuO nanorods with high hydrogen storage ability. *J. Nanomater.* **2011**, *201*, 1–6. [[CrossRef](#)]
10. Zhu, H.; Wang, J.; Xu, G. Fast Synthesis of Cu<sub>2</sub>O hollow microspheres and their application in DNA biosensor of hepatitis B virus. *Cryst. Growth Des.* **2009**, *9*, 633–638. [[CrossRef](#)]
11. Saravanan, S.; Sivasankar, T. Effect of ultrasound power and calcination temperature on the sonochemical synthesis of copper oxide nanoparticles for textile dyes treatment. *Environ. Prog. Sustain. Energy* **2016**, *35*, 669–679. [[CrossRef](#)]
12. Zhang, J.; Liu, J.; Peng, Q.; Wang, X.; Li, Y. Nearly monodisperse Cu<sub>2</sub>O and CuO nanospheres: Preparation and applications for sensitive gas sensors. *Chem. Mater.* **2006**, *18*, 867–871. [[CrossRef](#)]
13. Pan, L.; Zou, J.-J.; Zhang, T.; Wang, S.; Li, Z.; Wang, L.; Zhang, X. Cu<sub>2</sub>O film via hydrothermal redox approach: Morphology and photocatalytic performance. *J. Phys. Chem. C* **2014**, *118*, 16335–16343. [[CrossRef](#)]
14. Wang, Z.; Wang, H.; Wang, L.; Pan, L. Controlled synthesis of Cu<sub>2</sub>O cubic and octahedral nano- and microcrystals. *Cryst. Res. Technol.* **2009**, *44*, 624–628. [[CrossRef](#)]
15. Gou, L.; Murphy, C.J. Solution-phase synthesis of Cu<sub>2</sub>O nanocubes. *Nano Lett.* **2003**, *3*, 231–234. [[CrossRef](#)]
16. Bhosale, M.A.; Bhanage, B.M. A simple approach for sonochemical synthesis of Cu<sub>2</sub>O nanoparticles with high catalytic properties. *Adv. Powder Technol.* **2016**, *27*, 238–244. [[CrossRef](#)]
17. Wang, W.-W.; Zhu, Y.-J.; Cheng, G.-F.; Huang, Y.-H. Microwave-assisted synthesis of cupric oxide nanosheets and nanowhiskers. *Mater. Lett.* **2006**, *60*, 609–612. [[CrossRef](#)]
18. Swarnkar, R.K.; Singh, S.C.; Gopal, R. Effect of aging on copper nanoparticles synthesized by pulsed laser ablation in water: Structural and optical characterizations. *Bull. Mater. Sci.* **2011**, *34*, 1363–1369. [[CrossRef](#)]
19. Khayati, G.R.; Nourafkan, E.; Karimi, G.; Moradgholi, J. Synthesis of cuprous oxide nanoparticles by mechanochemical oxidation of copper in high planetary energy ball mill. *Adv. Powder Technol.* **2013**, *24*, 301–305. [[CrossRef](#)]
20. Kuppasamy, P.; Ilavenil, S.; Srigopalram, S.; Maniam, G.P.; Yusoff, M.M.; Govindan, N.; Choi, K.C. Treating of palm oil mill effluent using *Commelina nudiflora* mediated copper nanoparticles as a novel bio-control agent. *J. Clean. Prod.* **2017**, *141*, 1023–1029. [[CrossRef](#)]
21. Ghorbani, H.R. Biological and non-biological methods for fabrication of copper nanoparticles. *Chem. Eng. Commun.* **2015**, *202*, 1463–1467. [[CrossRef](#)]
22. Nagar, N.; Devra, V. Green synthesis and characterization of copper nanoparticles using *Azadirachta indica* leaves. *Mater. Chem. Phys.* **2018**, *213*, 44–51. [[CrossRef](#)]
23. Angajala, G.; Pavan, P.; Subashini, R. One-step biofabrication of copper nanoparticles from *Aegle Marmelos correa* aqueous leaf extract and evaluation of its anti-inflammatory and mosquito larvicidal efficacy. *RSC Adv.* **2014**, *4*, 51459–51470. [[CrossRef](#)]
24. Gunalan, S.; Sivaraj, R.; Venckatesh, R. *Aloe barbadensis* Miller mediated green synthesis of mono-disperse copper oxide nanoparticles: Optical properties. *Spectrochim. Acta Part A Mol. Biomol. Spectrosc.* **2012**, *97*, 1140–1144. [[CrossRef](#)] [[PubMed](#)]
25. Sivaraj, R.; Rahman, P.K.S.M.; Rajiv, P.; Narendhran, S.; Venckatesh, R. Biosynthesis and characterization of *Acalypha indica* mediated copper oxide nanoparticles and evaluation of its antimicrobial and anticancer activity. *Spectrochim. Acta Part A Mol. Biomol. Spectrosc.* **2014**, *129*, 255–258. [[CrossRef](#)]

26. Ghidan, A.Y.; Al-Antary, T.M.; Awwad, A.M. Green synthesis of copper oxide nanoparticles using *Punica granatum* peels extract: Effect on green peach Aphid. *Environ. Nanotechnol. Monit. Manag.* **2016**, *6*, 95–98. [[CrossRef](#)]
27. Yallappa, S.; Manjanna, J.; Sindhe, M.A.; Satyanarayan, N.D.; Pramod, S.N.; Nagaraja, K. Microwave assisted rapid synthesis and biological evaluation of stable copper nanoparticles using *T. arjuna* bark extract. *Spectrochim Acta A Mol. Biomol. Spectrosc.* **2013**, *110*, 108–115. [[CrossRef](#)]
28. Khatami, M.; Heli, H.; Jahani, P.M.; Marcos, H.A.; Nobre, A.L. Copper/copper oxide nanoparticles synthesis using *Stachys lavandulifolia* and its antibacterial activity. *IET Nanobiotechnol.* **2017**, *11*, 709–713. [[CrossRef](#)]
29. Viswadevarayalu, A.; Ramana, P.V.; Kumar, G.S.; Sumalatha, J.; Reddy, S.A. Fine ultrasmall copper nanoparticle (UCuNPs) synthesis by using *Terminalia bellirica* fruit extract and its antimicrobial activity. *J. Clust. Sci.* **2016**, *27*, 155–168. [[CrossRef](#)]
30. Kumar, B.; Smita, K.; Cumbal, C.; Debut, A.; Angulo, Y. Biofabrication of copper oxide nanoparticles using Andean blackberry (*Rubus glaucus* Benth.) fruit and leaf. *J. Saudi Chem. Soc.* **2017**, *21*, S475–S480. [[CrossRef](#)]
31. Kodahl, N. Sacha inchi (*Plukenetia volubilis* L.)—From lost crop of the Incas to part of the solution to global challenges? *Planta* **2020**, *251*, 80. [[CrossRef](#)] [[PubMed](#)]
32. Nascimento, A.K.L.; Melo-Silveira, R.F.; Dantas-Santos, N.; Fernandes, J.M.; Zucolotto, S.M.; Rocha, H.A.O.; Scortecci, K.C. Antioxidant and antiproliferative activities of leaf extracts from *Plukenetia volubilis* Linneo (Euphorbiaceae). *Evid. Based Complement. Altern. Med.* **2013**, *2013*, 950272. [[CrossRef](#)] [[PubMed](#)]
33. Wang, S.; Zhub, F.; Kakuda, Y. Sacha inchi (*Plukenetia volubilis* L.): Nutritional composition, biological activity, and uses. *Food Chem.* **2018**, *265*, 316–328. [[CrossRef](#)] [[PubMed](#)]
34. Kumar, B.; Smita, K.; Cumbal, C.; Debut, A. Synthesis of silver nanoparticles using Sacha inchi (*Plukenetia volubilis* L.) leaf extracts. *Saudi J. Biol. Sci.* **2014**, *21*, 605–609. [[CrossRef](#)]
35. Kumar, B.; Smita, K.; Cumbal, C.; Debut, A. Sacha inchi (*Plukenetia volubilis* L.) oil for one pot synthesis of silver nanocatalyst: An ecofriendly approach. *Ind. Crop. Prod.* **2014**, *58*, 238–243. [[CrossRef](#)]
36. Kumar, B.; Smita, K.; Cumbal, C.; Debut, A. One pot synthesis and characterization of gold nanocatalyst using Sacha inchi (*Plukenetia volubilis*) oil: Green approach. *J. Photochem. Photobiol. B Biol.* **2016**, *158*, 55–60. [[CrossRef](#)]
37. Kumar, B.; Smita, K.; Cumbal, C.; Debut, A. Sacha inchi (*Plukenetia volubilis* L.) shell biomass for synthesis of silver nanocatalyst. *J. Saudi Chem. Soc.* **2017**, *21*, S293–S298. [[CrossRef](#)]
38. Kumar, B.; Smita, K.; Sánchez, E.; Stael, C.; Cumbal, C. Andean Sacha inchi (*Plukenetia volubilis* L.) shell biomass as new biosorbents for Pb<sup>2+</sup> and Cu<sup>2+</sup> ions. *Ecol. Eng.* **2016**, *93*, 152–158. [[CrossRef](#)]
39. Abboud, Y.; Saffaj, T.; Chagraoui, A.; El Bouari, A.; Brouzi, K.; Tanane, O.; Ihssane, B. Biosynthesis, characterization and antimicrobial activity of copper oxide nanoparticles (CONPs) produced using brown alga extract (*Bifurcaria bifurcata*). *Appl. Nanosci.* **2014**, *4*, 571–576. [[CrossRef](#)]
40. Borgohain, K.; Murase, N.; Mahamuni, S. Synthesis and properties of Cu<sub>2</sub>O quantum particles. *J. Appl. Phys.* **2002**, *92*, 1292–1297. [[CrossRef](#)]
41. Bhattacharjee, S. DLS and zeta potential—What they are and what they are not? *J. Control. Release* **2016**, *235*, 337–351. [[CrossRef](#)] [[PubMed](#)]
42. Meghana, S.; Kabra, P.; Chakraborty, S.; Padmavathy, N. Understanding the pathway of antibacterial activity of copper oxide nanoparticles. *RSC Adv.* **2015**, *5*, 12293–12299. [[CrossRef](#)]
43. Lin, H.; Huang, C.P.; Li, W.; Ni, C.; Shah, S.I.; Tseng, Y.H. Size dependency of nanocrystalline TiO<sub>2</sub> on its optical property and photocatalytic reactivity exemplified by 2-chlorophenol. *Appl. Catal. B Environ.* **2006**, *68*, 1–11. [[CrossRef](#)]
44. Moniri, S.; Ghoranneviss, M.; Hantehzadeh, M.R.; Asadabad, M.A. Synthesis and optical characterization of copper nanoparticles prepared by laser ablation. *Bull. Mater. Sci.* **2017**, *40*, 37–43. [[CrossRef](#)]
45. Fathima, J.B.; Pugazhendhi, A.; Oves, M.; Venis, R. Synthesis of eco-friendly copper nanoparticles for augmentation of catalytic degradation of organic dyes. *J. Mol. Liq.* **2018**, *260*, 1–8. [[CrossRef](#)]

